Muon Monte Carlo: a new high-precision tool for muon propagation through matter

Dmitry Chirkin[1,2], **Wolfgang Rhode**[2]
chirkin@physics.berkeley.edu
rhode@wpos7.physik.uni-wuppertal.de

[1]*University of California at Berkeley, USA*
[2]*Bergische Universität Gesamthochschule Wuppertal, Germany*

Abstract

Propagation of muons through large amounts of matter is a crucial necessity for analysis of data produced by muon/neutrino underground experiments. A muon may sustain hundreds of interactions before it is seen by the experiment. Since a small uncertainty, introduced hundreds of times may lead to sizable errors, requirements on the precision of the muon propagation code are very stringent. A new tool for propagating muon and tau charged leptons through matter that is believed to meet these requirements is presented here. The latest formulae available for the cross sections were used and the reduction of the calculational errors to a minimum was our top priority. The tool is a very versatile program written in an object-oriented language environment (Java). It supports many different optimization (parametrization) levels. The fully parametrized version is as fast or even faster than the competition. On the other hand, the slowest version of the program that does not make use of parametrizations, is fast enough for many tasks if queuing or SYMPHONY environments with large number of connected computers are used. An overview of the program is given and some results of its application are discussed.

mmc code homepage is
http://area51.berkeley.edu/~dima/work/MUONPR/
mmc code available at
http://area51.berkeley.edu/~dima/work/MUONPR/BKP/mmc.tgz

1 Introduction

In order to observe atmospheric and cosmic neutrinos with a large underground detector (e.g. AMANDA [1]), one needs to isolate their signal from the 3-5 orders of magnitude larger signal from the background of atmospheric muons. Methods that do this have been designed and proven viable [2]. In order to prove that these methods work and to derive indirect results such as the spectral index of atmospheric muons, one needs to compare data to the results of the computer simulation. Such a simulation normally contains three parts: propagation of the measured flux of the cosmic particles from the top of the atmosphere down to the surface of the ground (ice, water); propagation of the atmospheric muons from the surface down to and through the detector; generation of the Cerenkov photons emanating from the muon tracks in the vicinity of the detector and their interaction with the detector components. The first part is normally called *generator*, since it generates muon flux at the ground surface; the second is *propagator*; and the third simulates the detector interaction with the passing muons. Mainly two generators were used so far (by AMANDA): basiev and CORSIKA [3]. Results and method of using CORSIKA as a generator in a neutrino detector (AMANDA) were discussed in our previous contribution [4]. Several muon propagation Monte Carlo programs were used with different degrees of success as propagators. Some are not suited for applications which require the code to propagate muons in a large energy range (e.g. mudedx), the others seem to work in only some of the interesting energy range ($E > 1$ TeV, propmu) [5]. Most of the programs use cross section formulae, whose precision has been improved since their writing. For some applications, one would also like to use the code for the propagation of muons that contain $100 - 1000$ interactions along their track, so the precision of each step should be sufficiently high and the computational errors should accumulate as slowly as possible. Significant discrepancies between the muon propagation codes we tested were observed, believed to be mostly due to algorithm errors. This motivated writing of a new code that would reduce calculational errors to minimum, leaving only those uncertainties that come from the imperfect knowledge of the cross sections. Here we present a new tool (Muon Monte Carlo: MMC), designed to meet this goal.

2 Description of the code

The primary design goals of MMC were uncompromising computational precision and code clarity. It was decided that the program should be written in JAVA, since JAVA is an object-oriented programming language (for best code readability) and has consistent behavior across many platforms. MMC consists of pieces of code (classes), each contained in a separate file. These pieces fulfill their separate tasks and are combined in a structured way (Fig. 1). This simplifies code maintenance and introduction of changes/corrections to the cross section formulae. It is also very straightforward to even "plug in" new cross sections, if necessary. Writing in an object-oriented language allows several instances of the program to be created and accessed simultaneously. This is useful for simulating the behavior of the e.g. neutrino detectors, where different conditions apply above, inside and below the detector.

The code evaluates many cross-section integrals, as well as two tracking integrals. All integral evaluations are done by the Romberg method of the 5th order (by default) [6] with a variable substitution (mostly log-exp). If an upper limit of an integral is an unknown (that depends on a random number), an approximation to that limit is found during normalization integral evaluation, and then refined by Newton-Raphson method combined with bisection [6].

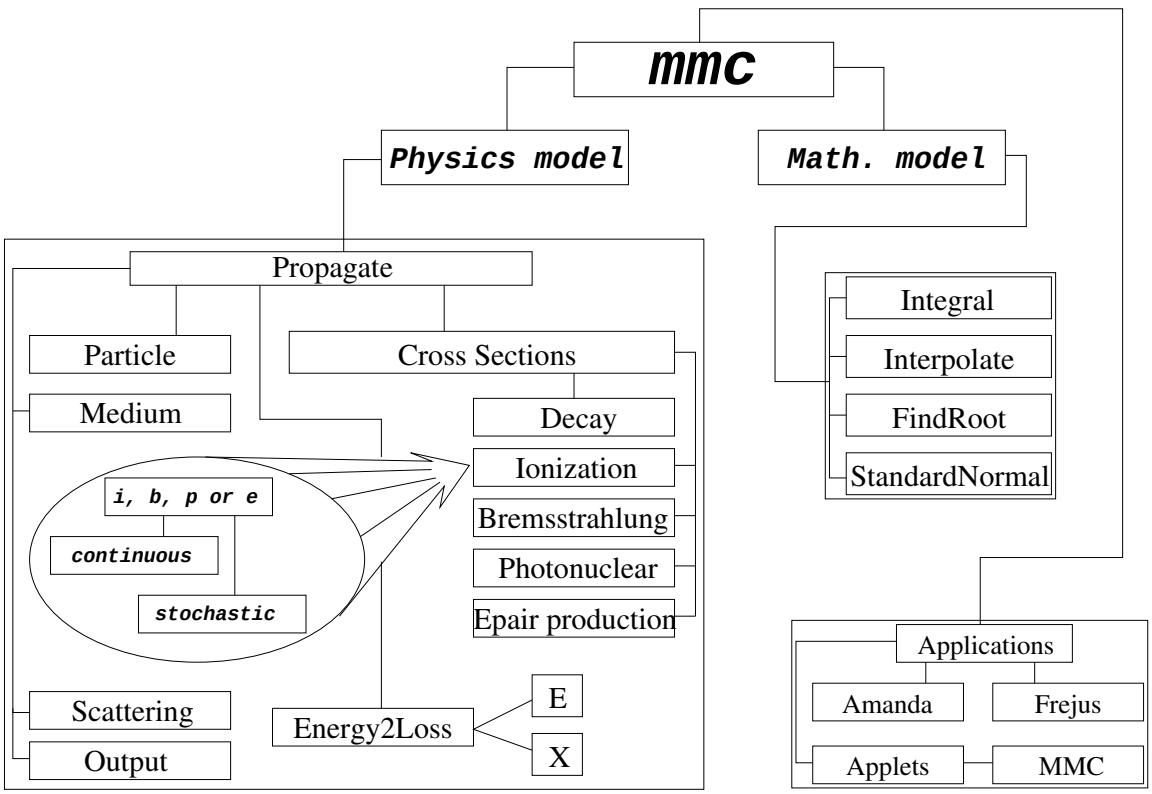

Fig. 1: MMC structure

Originally, the program was designed to be used in the Massively Parallel Network Computing (SYMPHONY) [10] framework, therefore computational speed was considered only a secondary issue. However, parametrization and interpolation routines were implemented for all integrals. These are both polynomial and rational function interpolation routines spanned over varying number of points (5 by default) [6]. Inverse interpolation is implemented for root finding (i.e. when $x(f)$ is interpolated to solve $f(x) = y$). Two dimensional interpolations are implemented as two consecutive one-dimensional ones. It is possible to turn parametrizations on or off for each integral separately at program initialization. The default energy range in which parametrized formulae will work was chosen to be from 105.7 MeV (the muon rest mass) to 10^{14} MeV and the program was tested to work with much higher setting for the higher energy cutoff. With full optimization (parametrizations) this code is at least as fast or even faster than the competition.

Generally, as a muon travels through matter, it loses energy due to ionization losses, bremsstrahlung, photo-nuclear interaction and pair production. Formulae for the cross sections were taken from the recent contribution [7]. These formulae are claimed to be valid to within about 1%. All of the energy losses have continuous and stochastic components, the division between which is superficial and is chosen in the program by selecting an energy cut (e_{cut}) or a relative energy loss cut (v_{cut}). In the following text v_{cut} and e_{cut} are considered to be interchangable and related by $e_{cut} = v_{cut}E$ (even though only one of them is a constant). Ideally, all losses should be treated stochastically. However, that would bring the number of separate energy loss events to a very large value, since the probability of such events to occur diverges as $1/E_{lost}$ for the bremsstrahlung losses, as the lost energy approaches zero, and even faster than that for the other losses. In fact, the only reason this large number is not infinity is existence of kinematic cutoffs (larger than some e_0) for all diverging cross sections. A good choice of v_{cut} for the propagation of atmospheric muons should lie in the

range (0.05 - 0.1) [8]. For monoenergetic beams of muons, v_{cut} may have to be chosen to be high as $10^{-3} - 10^{-4}$.

2.1 Tracking formulae

Let the continuous part of the energy losses (a sum of all energy losses, integrated from zero to e_{cut}) be described by a function f(E):

$$-\frac{dE}{dx} = f(E).$$

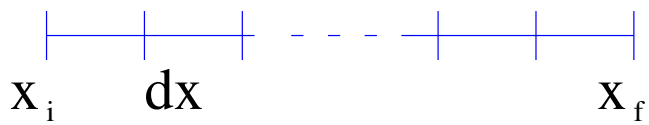

Fig. 2: derivation of tracking formulae

The stochastic part of the losses is described by the function $\sigma(E)$, which is a probability for any energy loss event (with lost energy $> e_{cut}$) to occur along a path of 1 cm. Consider the particle path from one interaction to the next consisting of small intervals (Fig. 2). On each of these small intervals probability of interaction is $dP(E(x_i)) = \sigma(E(x_i))dx$. It is easy to derive an expression for the final energy on this step as a function of the random number ξ. Probability to completely avoid stochastic processes on an interval (x_i;x_f) and then suffer a catastrophic loss on dx at x_f is

$$(1 - dP(E(x_i))) \cdot ... \cdot (1 - dP(E(x_f))) \cdot dP(E(x_f))$$

$$= \exp(-dP(E(x_i))) \cdot ... \cdot \exp(-dP(E(x_f))) \cdot dP(E(x_f))$$

$$= \exp\left(-\int_{E_i}^{E_f} dP(E(x))\right) \cdot dP(E(x_f))$$

$$= d_f\left(-\exp(-\int_{E_i}^{E_f} \frac{\sigma(E)}{-f(E)} \cdot dE)\right) = d(-\xi), \quad \xi \in (0;1]$$

To find the final energy on each step the above equation is solved for E_f:

$$\int_{E_i}^{E_f} \frac{\sigma(E)}{-f(E)} \cdot dE = -\log(\xi) \quad \text{(energy integral).}$$

This equation has a solution if

$$\xi > \xi_0 = \exp\left(-\int_{e_{low}}^{E_i} \frac{\sigma(E)}{f(E)} \cdot dE\right).$$

Here e_{low} is a low energy cutoff, below which the muon is considered to be lost. Please note, that $f(E)$ is always positive due to ionization losses (unless $e_{cut} \sim I(Z)$). $\sigma(E)$ is also always positive because it includes the positive decay probability. If $\xi < \xi_0$, the particle is stopped and its energy is set to e_{low}. The corresponding displacement for all ξ can be found from

$$x_f = x_i - \int_{E_i}^{E_f} \frac{dE}{f(E)} \quad \text{(tracking integral).}$$

2.2 Continuous randomization It was found that for higher v_{cut} muon spectra do not look compact (Fig. 3). In fact, there is a large peak (at E_{peak}) that collects all particles that did not suffer stochastic losses followed by the main spectrum distribution separated from the peak by at least the value of $v_{cut}E_{peak}$ (the smallest stochastic loss). The appearance of the peak and its prominence are governed by v_{cut}, initial energy − propagation distance ratio and the binning of the final energy spectrum histogram. In order to be able to approximate the real spectra with even large v_{cut} and to study the systematic effect at a large v_{cut}, a "continuous randomization" feature was introduced.

For a fixed v_{cut} or e_{cut} a particle is propagated until the algorithm discussed above finds an interaction point, i.e. a point where the particle loses more than the cutoff energy. The average value of the energy decrease due to continuous energy losses is evaluated according to the energy integral formula above. There will be some fluctuations in this energy loss, which are discarded by the formula. Let's assume there is a cutoff for all processes at some small $e_0 \ll e_{cut}$. Then the probability $p(e;E)$ for a process with $e_0 < e_{lost} < e_{cut}$ on the distance dx is normalizable to 1. Let's choose dx so small that

$$p_0 = \int_{e_0}^{e_{cut}} p(e;E)\, de \cdot dx \ll 1$$

Then the probability to not have any losses is $1-p_0$, and the probability to have two or more separate losses is negligible. The standard deviation of the energy loss on dx from the average value

$$< e >= \int_{e_0}^{e_{cut}} e \cdot p(e;E)\, de \cdot dx$$

is then $< (\Delta e)^2 >=< e^2 > - < e >^2$, where

$$< e^2 >= \int_{e_0}^{e_{cut}} e^2 \cdot p(e;E)\, de \cdot dx$$

If v_{cut} or e_{cut} used for the calculation is sufficiently small, the distance $x_f - x_i$ determined by the energy and tracking integrals is so small that the average energy loss $E_i - E_f$ is also small (as compared to the initial energy E_i). We therefore may assume $p(e;E) \simeq p(e;E_i)$, i.e. the energy loss distributions on the small intervals dx_n that sum up to the $x_f - x_i$, is the same for all intervals. Since the total energy loss $E_i - E_f = \sum e_n$, the central limit theorem can be applied, and the final energy loss distribution will be Gaussian with the average $\Delta E = E_i - E_f$ and width

$$< (\Delta(\Delta E))^2 >= \sum_n \left(< e_n^2 > - < e_n >^2\right)$$

$$= \sum_n \left[\left(\int_{e_0}^{e_{cut}} e_n^2 \cdot p(e_n;E_i)\, de_n \right) dx_n - \left(\int_{e_0}^{e_{cut}} e_n \cdot p(e_n;E_i)\, de_n \right)^2 dx_n^2 \right]$$

$$\simeq \int_{x_i}^{x_f} dx \cdot \left(\int_{e_0}^{e_{cut}} e^2 \cdot p(e;E(x))\, de \right) - \int_{x_i}^{x_f} dx \cdot \left(\int_{e_0}^{e_{cut}} e \cdot p(e;E(x))\, de \right)^2 dx$$

Here E_i was replaced with average expectation value of energy at x, $E(x)$. As $dx \to 0$, the second term disappears. The lower limit of the integral over e can be replaced with zero, since all of the cross sections diverge slower than $1/e^3$. Then,

$$< (\Delta(\Delta E))^2 >\simeq \int_{x_i}^{x_f} \frac{dE}{-f(E)} \cdot \left(\int_0^{e_{cut}} e^2 \cdot p(e;E)\, de \right)$$

This formula is applicable for small v_{cut}, as seen from the derivation. Energy spectra calculated with "continuous randomization" converge faster than those without (see Fig. 4-5).

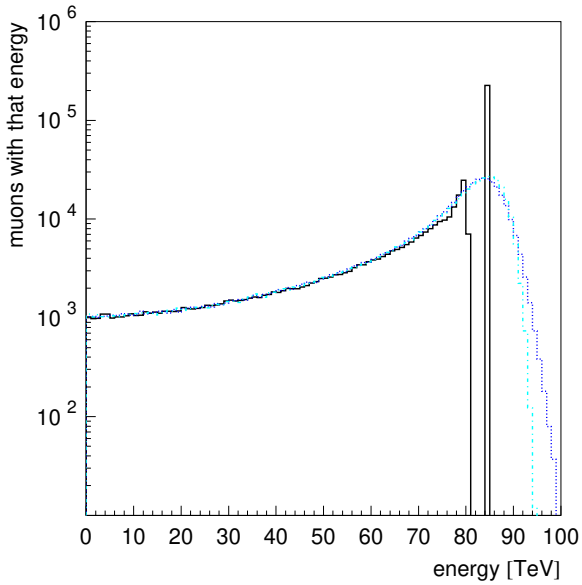

Fig. 3: Distribution of the final energy of the muons that crossed 300 m of Fréjus Rock with initial energy 100 TeV: $v_{cut} = 0.05$ (solid), $v_{cut} = 10^{-4}$ (dashed-dotted), $v_{cut} = 0.05$ and "cont" option (dotted)

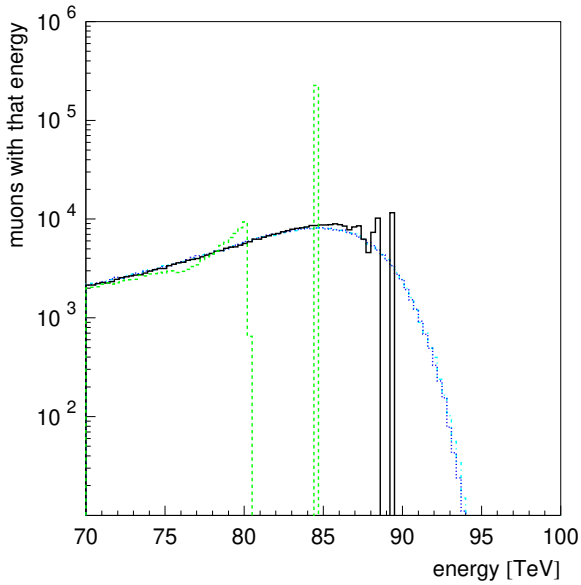

Fig. 4: A close-up on the Fig. 3: $v_{cut} = 0.05$ (dashed), $v_{cut} = 0.01$ (solid), $v_{cut} = 10^{-3}$ (dotted), $v_{cut} = 10^{-4}$ (dashed-dotted)

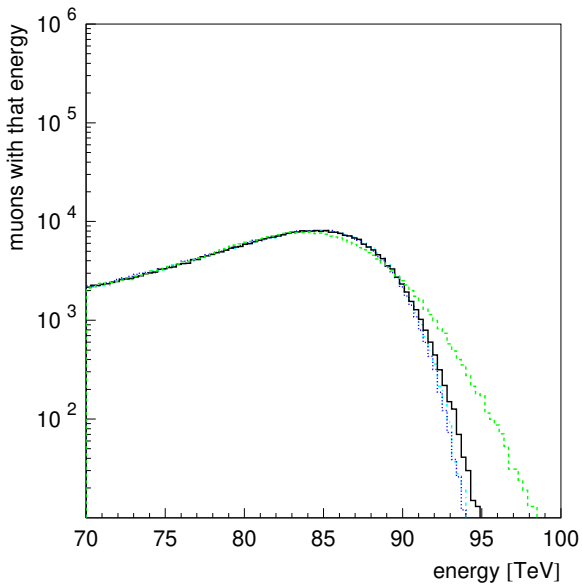

Fig. 5: Same as in Fig. 4, but with "cont" option enabled

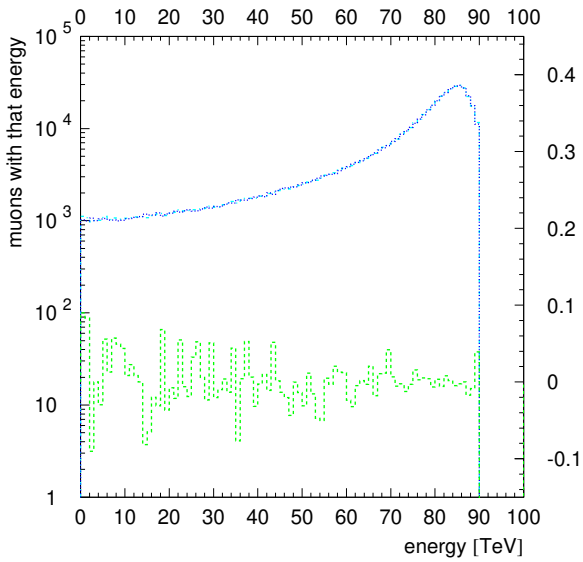

Fig. 6: Comparison of paramerized (dashed-dotted) with exact (non-parametrized, dotted) versions for $v_{cut} = 0.01$. Also shown is the relative difference of the curves.

3 Errors

All cross-section integrals are evaluated to the relative precision of 10^{-6}, the tracking integrals are functions of these, so their precision was set to a higher value of 10^{-5}. To check the precision

of interpolation routines, results of running with parametrizations enabled were compared to those with parametrizations disabled. Fig. 7 shows relative energy losses for ice due to different mechanisms. Decay energy loss is shown here only for comparison and is evaluated by multiplying the probability of decay by the energy of the particle. In the region below 1 GeV bremsstrahlung energy loss has a double cutoff structure. This is due to a difference in the kinematic restrictions for muon interaction with oxygen and hydrogen atoms. A cutoff (for any process) is a complicated structure to parametrize and with only a few parametrization grid points in the cutoff region, interpolation errors $(e_{pa} - e_{np})/e_{pa}$ may become quite high, reaching 100% right below the cutoff, where the interpolation routines give non-zero values, whereas the exact values are zero. But since the energy losses due to either bremsstrahlung, photonuclear process or pair production are very small near the cutoff in comparison to the sum of all losses (mostly ionization energy loss), this big relative error results in a much smaller increase of the relative error of the total energy losses (Fig. 8). Because of that, parametrization errors never exceed 10^{-4} - 10^{-3}, for the most part being even much smaller (10^{-6} - 10^{-5}), as one can estimate from the plot. These errors are much smaller than the uncertainties in the formulae for the cross sections. Now the question arises whether this precision is sufficient to propagate muons with hundreds of interactions along their way. Fig. 6 is one of the examples that demonstrate that it is sufficient: the final energy distribution did not change after enabling parametrizations.

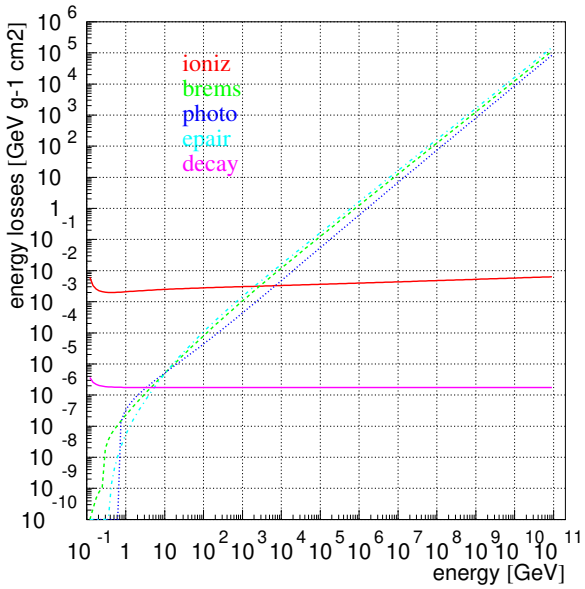

Fig. 7: ioniz (upper solid curve), brems (dashed), photo (dotted), epair (dashed-dotted) and decay (lower solid curve) losses in ice

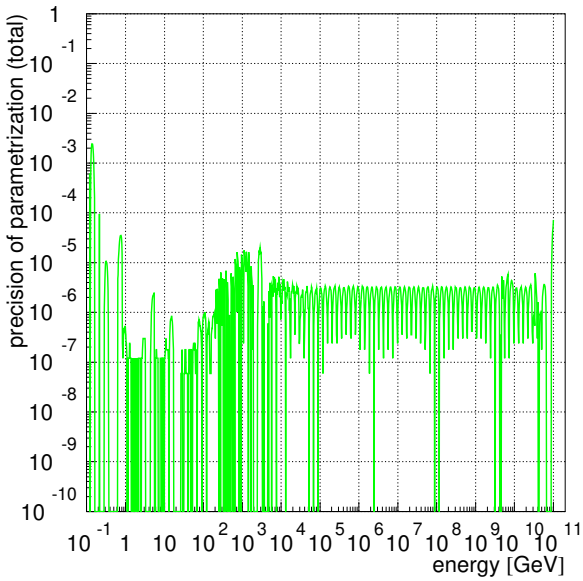

Fig. 8: Interpolation precision $(e_{pa} - e_{np})/e_{pa}$

MMC has a low energy cutoff e_{low} below which the muon is considered to be lost. By default it is equal to the mass of the muon, but can be changed to any higher value. This cutoff enters the calculation in several places, most notably in the initial evaluation of the energy integral. To determine the random number ξ_0 below which the particle is considered stopped, the energy integral is first evaluated from E_i to e_{low}. It is also used in the parametrization of the energy and tracking integrals, since they are evaluated from this value to E_i and E_f, and then the interpolated value for E_f is subtracted from that for E_i. Fig. 9 demonstrates the independence of MMC from the value of

e_{low}. For the curve with $e_{low} = m_\mu$ integrals are evaluated in the range 105.7 MeV − 100 TeV, i.e. over six orders of magnitude, and they are as precise as those calculated for the curve with e_{low}=10 TeV, with integrals being evaluated over only one order of magnitude.

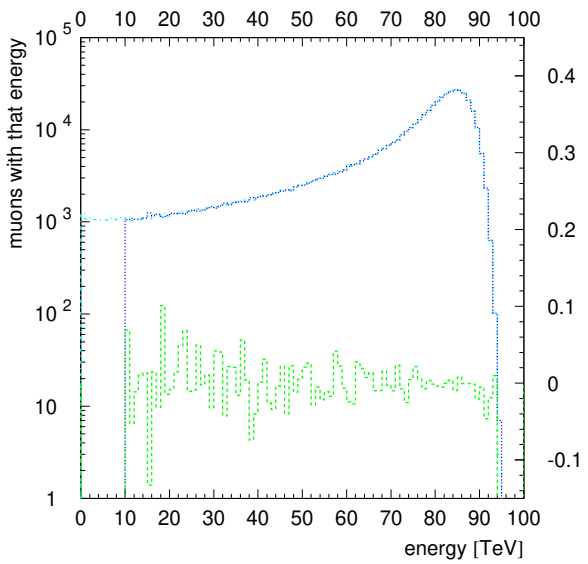

Fig. 9: Comparison of $e_{low} = m_\mu$ (dotted-dashed) with e_{low}=10 TeV (dotted). Also shown is the relative difference of the curves.

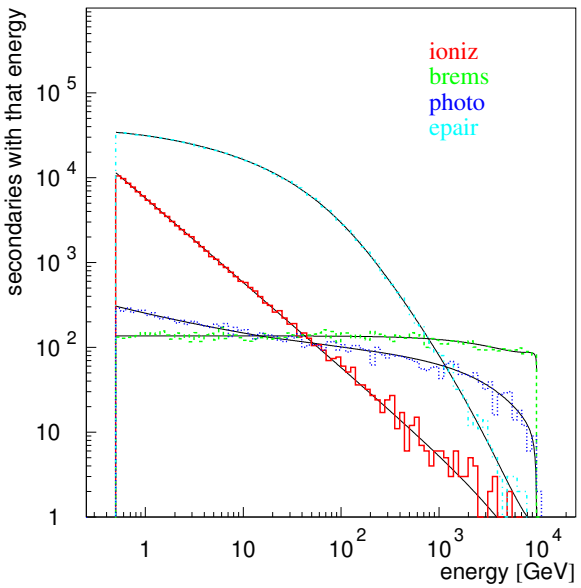

Fig. 10: ioniz (upper solid curve), brems (dashed), photo (dotted), epair (dashed-dotted) spectra for E_μ=10 TeV in the Fréjus rock

Fig. 10 demonstrates the spectra of secondaries (delta electrons, bremsstrahlung photons, excited nuclei and electron pairs) produced by the muon, which energy is kept constant at 10 TeV. The thin lines behind the histograms are the probability functions (roughly cross sections) used in the calculation. They have been corrected to fit the logarithmically binned histograms (multiplied by the size of the bin which is proportional to abscissa, i.e. energy). While the agreement is trivial from the Monte Carlo point of view, it demonstrates that the computational algorithm is correct.

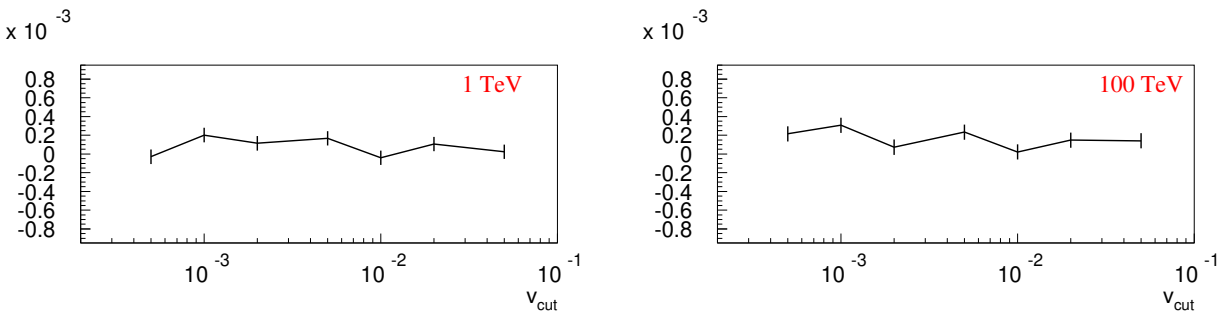

Fig. 11

Fig. 11 shows the relative deviation of the average final energy of the $4 \cdot 10^6$ 1 TeV and 100 TeV muons propagated through 100 m of Fréjus rock with the abscissa setting for v_{cut}, from the final energy obtained with $v_{cut} = 1$. Just like in [8] the distance was chosen small enough so that only a negligible number of muons stop, while big enough so that the muon suffers a big number of stochastic losses (> 10 for $v_{cut} \leq 10^{-3}$). All points should agree with the result for $v_{cut} = 1$,

since it should be equal to the integral of all energy losses, and averaging over the energy losses for $v_{cut} < 1$ is evaluating such an integral with the Monte Carlo method. There is a visible systematic shift $\lesssim 1 - 2 \cdot 10^{-4}$ (similar for other muon energies), which can be considered as another measure of the algorithm accuracy [8].

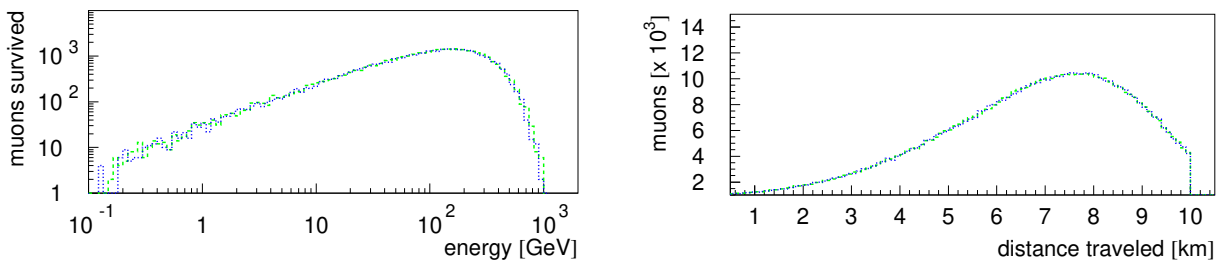

Fig. 12: 10^6 muons with energy 9 TeV propagated through 10 km of water: regular (dashed) vs. "cont" (dotted)

In case when almost all muons stop before passing the requested distance (see Fig. 12), even small algorithm errors may affect survival probabilities by a lot. The following table summarizes the survival probabilities of monochromatic muon beam of 10^6 muons with three initial energies (1 TeV, 9 TeV and 10^6 TeV) going through three distances (3 km, 10 km and 40 km) in water. One should note that these numbers are very sensitive to the formulae of cross sections used in the calculation; e.g. for the muons with energy 10^9 GeV propagated through 40 km the rates decrease 30 % when the default photonuclear cross section is replaced with the ZEUS parametrization (case number four from Sec. 6.3). However, the same set of formulae was used throughout the calculation. The errors of the values in the table are statistical and are $\lesssim \pm 0.001$.

v_{cut}	"cont"	1 TeV 3 km	9 TeV 10 km	10^6 TeV 40 km
0.2	no	0	0	0.153
0.2	yes	0.010	0.057	0.177
0.05	no	0	0.035	0.143
0.05	yes	0.045	0.039	0.139
0.01	no	0.030	0.037	0.142
0.01	yes	0.034	0.037	0.139
10^{-3}	no	0.034	0.037	0.140
10^{-3}	yes	0.034	0.037	0.135

The survival probabilities converge on the final value for $v_{cut} \lesssim 0.01$ in the first two columns. Using the "cont" version helped the convergence in the first column. However, the "cont" values departed from regular values more in the third column. The relative deviation (3.5%) can be used as an estimate of the continuous randomization algorithm precision (not calculational errors) in this case. One should note, however, that with the number of interactions $\gtrsim 10^3$ the continuous randomization approximation formula was applied $\gtrsim 10^3$ times. It explains why the value of "cont" version for $v_{cut} = 0.01$ is closer to the converged value of the regular version than for $v_{cut} = 10^{-3}$.

4 Results

The code was incorporated into the Monte Carlo chains of two detectors: Fréjus [9] and AMANDA [5]. In this section some general results are presented.

The energy losses plot was fitted to the function $dE/dx = a + bE$ (Fig. 13). The first two formulae for the photonuclear cross section (Sec. 6.3) can be fitted the best, all others lead to energy losses deviating more at higher energies from this simple linear formula; therefore the numbers given were evaluated using the first photonuclear cross section formula. In order to choose low and high energy limits correctly (to cover the maximum possible range of energies that could be comfortably fitted with a line), a χ^2 plot was generated and analysed (Fig. 14). It can be seen that χ^2 plot at the low energies goes down sharply, then levels out. This corresponds to the point where linear approximation starts to work. At high energies χ^2 rises monotonically. This means that a linear approximation, though valid, has to describe a growing energy range. An interval of energies from 20 GeV to 10^{11} GeV is chosen for the fit. The following table summarizes the found fits to a and b:

medium	a, $\frac{GeV}{mwe}$	b, $\frac{10^{-3}}{mwe}$	av. dev.	max. dev.
ice	0.259	0.357	3.7%	6.6%
fr. rock	0.231	0.429	3.0%	5.1%

The errors in the evaluation of a and b are in the last digit of the given number. However, if the lower energy boundary of the fitted region is raised and/or the upper energy boundary is lowered, each by an order of magnitude, a and b change by about 1%.

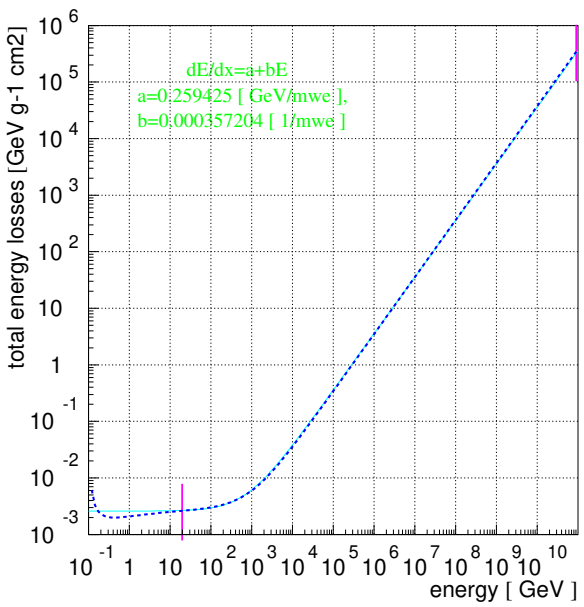

Fig. 13: Fit to the energy losses in ice

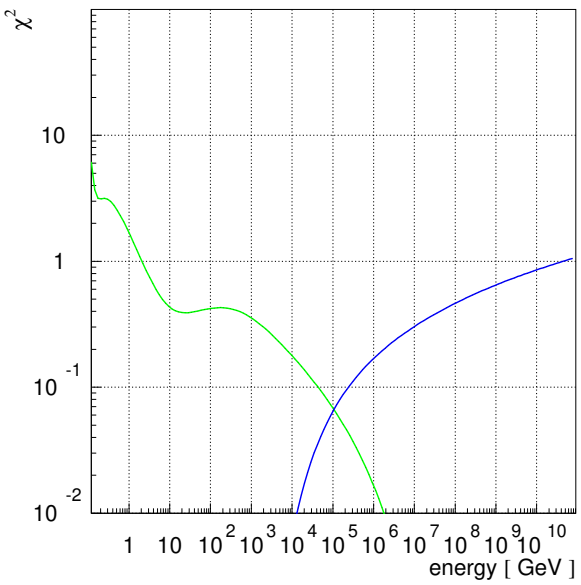

Fig. 14: χ^2 plot for energy losses in ice

To investigate the effect of stochastic processes, muons with energies 105.7 MeV - 10^{11} GeV were propagated to the point of their disappearance. $v_{cut} = 5 \cdot 10^{-3}$ was used in this calculation; using the version with the continuous randomization did not change the final numbers. Average final distance (range) for each energy was fitted to the solution of the energy loss equation $dE/dx = a + bE$:

$$x_f = \log(1 + E_i \cdot b/a)/b$$

(Fig. 15). The same analysis of the χ^2 plot as above was done in this case (Fig. 16). A region of initial energies from 20 GeV to 10^{11} GeV was chosen for the fit. The following table summarizes the results of these fits:

medium	a, $\frac{GeV}{mwe}$	b, $\frac{10^{-3}}{mwe}$	av. dev.
ice	0.268	0.470	3.0%
fréjus rock	0.218	0.520	2.8%

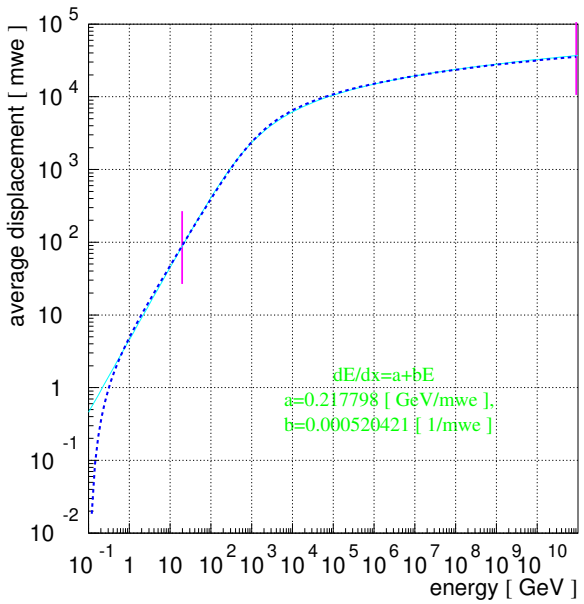

Fig. 15: Fit to the average range in Fréjus rock

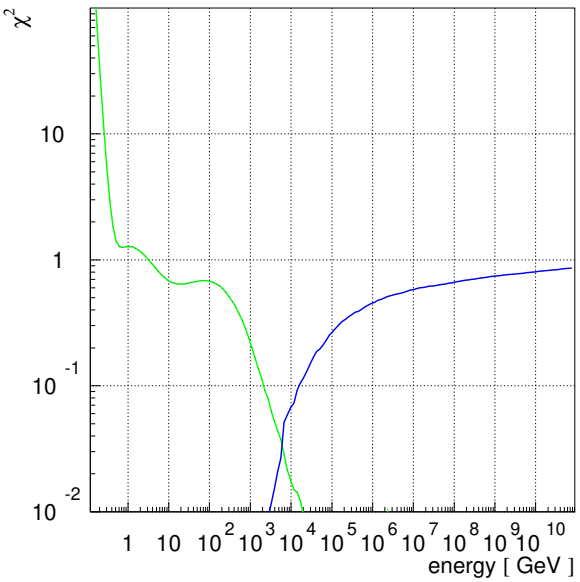

Fig. 16: χ^2 plot for average range in Fréjus rock

As the energy of the muon increases, it suffers more interactions before it is lost and the range distribution becomes more Gaussian-like (Fig. 17). It is obvious that the inclusion of stochastic processes into consideration leads in general to larger energy losses at higher energies than with only continuous processes and the center of gravity of the muon beam travels to a smaller distance.

5 Conclusions

A very versatile, clear-coded and easy-to-use Muon propagation Monte Carlo program (MMC) is presented. It is capable of propagating muon and tau leptons of energies from 105.7 MeV (muon rest mass, higher for tau) to 10^{11} GeV (or higher), which should be sufficient for the use as propagator in the simulations of the modern neutrino detectors. A very straightforward error control model is implemented, which results in computational errors being much smaller than uncertainties in the formulae used for evaluation of cross sections. It is very easy to "plug in" cross sections, modify them, or test their performance. The program was extended on many occasions to include new formulae or effects. MMC does all calculations and checks in three dimensions and takes into account Molière scattering on the atomic centers, which could be considered as the zeroth order approximation to true muon scattering since bremsstrahlung and pair production are effects that appear on top of such scattering. A more advanced angular dependence of the cross sections can be inserted at a later date, if necessary.

The MMC program was successfully incorporated into and used in the Monte Carlo chains of AMANDA and Fréjus experiments. We hope that the combination of precision, code clarity, speed and stability will make this program a useful tool in the research connected with high energy particles propagating through matter.

Also, a calculation of coefficients in the energy loss formula $dE/dx = a + bE$ is presented for both continuous and full (continuous and stochastic) energy loss treatments. The calculated coefficients apply in the energy range from 20 GeV to 10^{11} GeV with an average deviation from the linear formula of 3.7% and maximum of 6.6%.

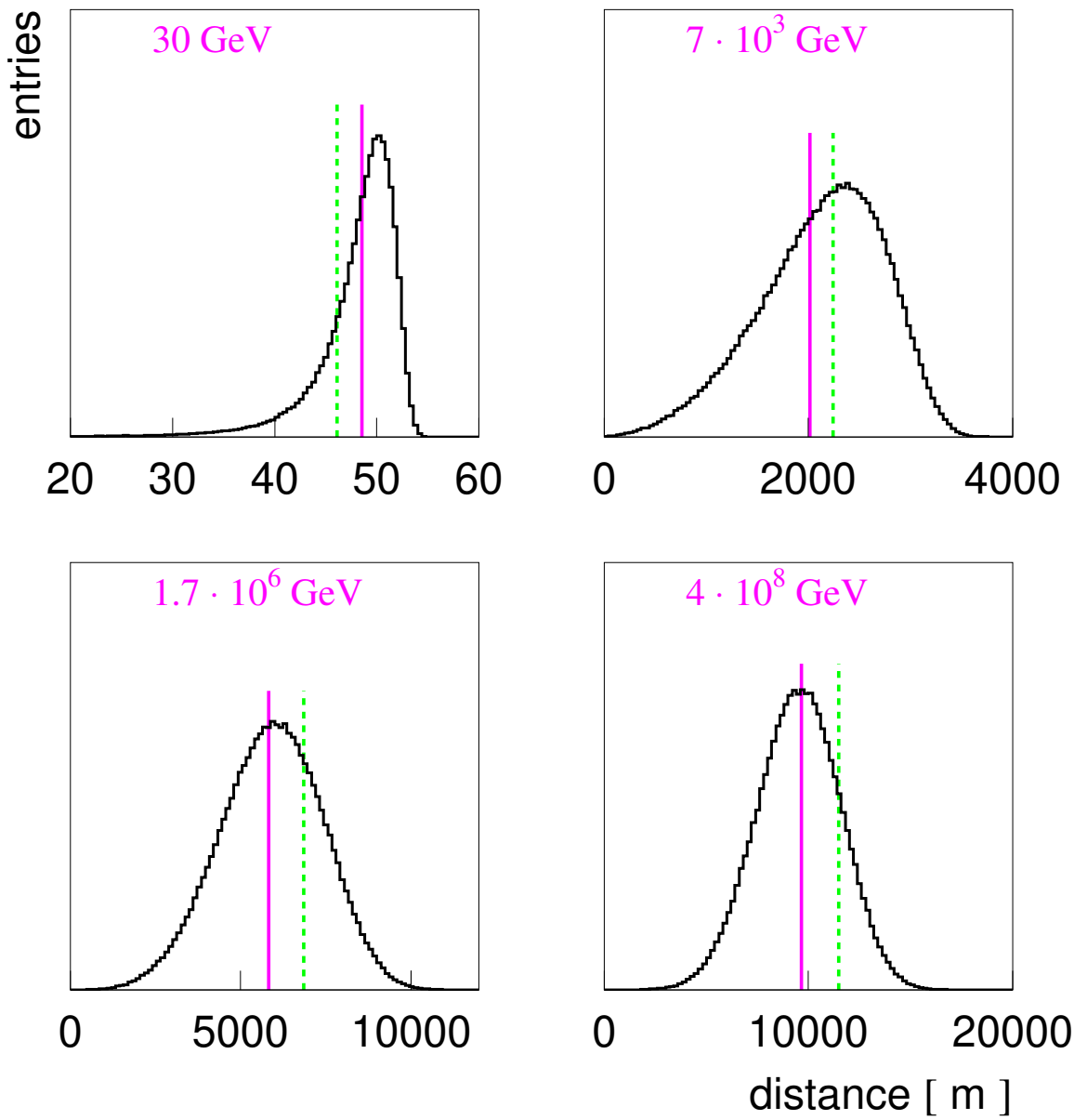

Fig. 17: Range distributions in Fréjus rock: solid line designates the value of the range evaluated with the second table (continuous and stochastic losses) and the broken line shows the range evaluated with the first table (continuous losses only).

6 Formulae

This section summarizes cross sections formulae used in MMC. In the formulae below E is the energy of the incident muon, while $\nu = vE$ is the energy of the secondary particle: knock on electron for ionization, photon for bremsstrahlung, virtual photon for photonuclear process and electron pair for the pair production. $\beta = v/c$ and $\gamma = (1-\beta^2)^{-1/2}$. μ is muon mass, $m = m_e$ is electron mass

and M is proton mass. Please refer to the next section for values of any constants appearing below. Most of the formulae in Sec. 6.1- 6.4 are taken directly from [7]

6.1 Ionization

A standard Bethe-Bloch equation given in [11] was modified for muon and tau charged leptons (massive particles with spin 1/2 different from electron) following the procedure outlined in [12]. The result is given below:

$$-\frac{dE}{dx} = Kz^2 \frac{Z}{A\beta^2}\left[\frac{1}{2}ln\left(\frac{2m_e\beta^2\gamma^2\nu\text{upper}}{I(Z)^2}\right) - \frac{\beta^2}{2}\left(1+\frac{\nu\text{upper}}{\nu\text{max}}\right) + \frac{1}{2}\left(\frac{\nu\text{upper}}{2E(1+1/\gamma)}\right)^2 - \frac{\delta}{2}\right]$$

$$\text{where} \quad \nu\text{max} = \frac{2m_e(\gamma^2-1)}{1+2\gamma\frac{m_e}{\mu}+\left(\frac{m_e}{\mu}\right)^2} \quad \text{and} \quad \nu\text{upper} = min(\nu\text{cut}, \nu\text{max})$$

The density correction δ is computed as for nonconductors:

$$\begin{aligned}
\delta &= 0, \quad \text{if } X < X_0 \\
\delta &= 2(\ln 10)X + C + a(X_1 - X)^m, \quad \text{if } X_0 \le X < X_1 \\
\delta &= 2(\ln 10)X + C, \quad \text{if } X \ge X_1 \quad \text{where} \quad X = log_{10}(\beta\gamma)
\end{aligned}$$

$$\frac{d^2N}{d\nu dx} = \frac{1}{2}Kz^2\frac{Z}{A}\frac{1}{\beta^2}\frac{1}{\nu^2}\left[1 - \beta^2\frac{\nu}{\nu\text{max}} + \frac{1}{2}\left(\frac{\nu}{E(1+1/\gamma)}\right)^2\right]$$

This formula, integrated from $\nu_{min} = \frac{1}{2m_e}\cdot\left(\frac{I(Z)}{\beta\gamma}\right)^2$ to ν_{upper}, gives the expression for energy loss above, less the density correction and β^2 terms (plus two more terms which vanish if $\nu_{min} \ll \nu_{upper}$).

6.2 Bremsstrahlung

According to [13], bremsstrahlung cross section may be represented by the sum of elastic component (σ_{el}, discussed in [14, 15]) and two inelastic components ($\Delta\sigma^{in}_{a,n}$)

$$\sigma = \sigma_{el} + \Delta\sigma^{in}_a + \Delta\sigma^{in}_n$$

6.2.1 Elastic Bremsstrahlung

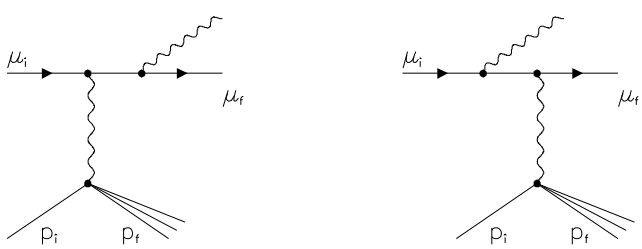

$$\sigma_{el}(E,v) = \frac{\alpha}{v}\left(2Z\frac{m}{\mu}r_e\right)^2\left(\frac{4}{3}-\frac{4}{3}v+v^2\right)\left[\ln\left[\frac{\mu}{\delta}\right]-\frac{1}{2}-\Delta^{el}_a-\Delta^{el}_n\right]$$

$$\text{where} \quad \delta \approx \frac{\mu^2\omega}{2E(E-\omega)}$$

is the minimum momentum transfer. The formfactors (atomic Δ^{el}_a and nuclear Δ^{el}_n) are

$$\begin{aligned}
\Delta^{el}_a(\delta) &= \ln\left[1+\frac{1}{\delta\sqrt{e}BZ^{-1/3}/m}\right] \\
\Delta^{el}_n(\delta) &= \ln\left[\frac{D_n}{1+\delta(D_n\sqrt{e}-2)/\mu}\right]; \qquad D_n = 1.54A^{0.27}
\end{aligned}$$

6.2.2 Inelastic Bremsstrahlung The effect of nucleus excitation can be evaluated as

$$\Delta_n^{in} = \frac{1}{Z}\Delta_n^{el};\ (Z \neq 1)$$

Bremsstrahlung on the atomic electrons can be described by the following diagrams:

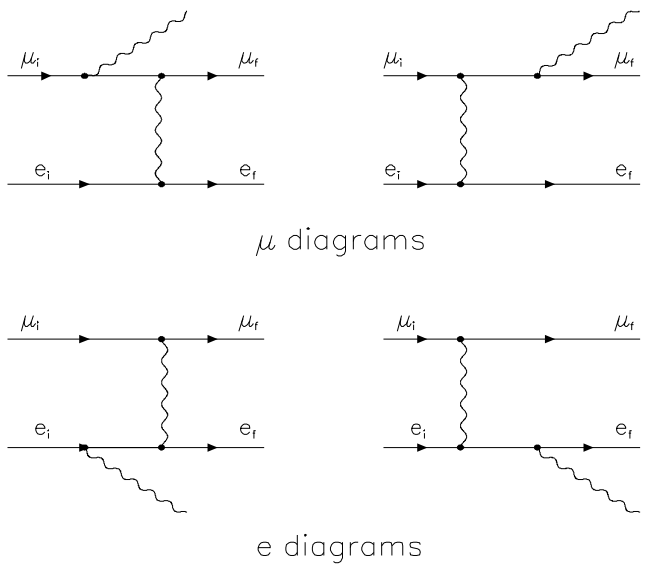

e-diagram is included with ionization losses (because of its sharp $1/v^2$ energy loss spectrum), as described in [16]

$$\Delta\frac{d^2N}{d\nu dx} = \left(\frac{d^2N}{d\nu dx}\right)_{I_0} \cdot \frac{\alpha}{2\pi}(a(2b+c) - b^2)$$

$$a = \log(1 + 2\nu/m_e), \quad b = \log((1 - \nu/\nu_{max})/(1 - \nu/E)),$$

$$c = \log((2\gamma(1 - \nu/E)m_e)/(m_\mu \nu/E))$$

Maximum energy lost by a muon is the same as in the pure ionization (knock-on) energy losses. Minimum energy is taken as $\nu_{min} = I(Z)$. In the above formula ν is the energy lost by the muon, i.e. the sum of energies transferred to both electron and photon. On the output all of this energy is assigned to the electron.

The contribution of the μ-diagram (included with bremsstrahlung) is discussed in [13]:

$$\Delta\sigma_a^{in}(E, v) \approx \frac{\alpha}{v}\left(2Z\frac{m}{\mu}r_e\right)^2\left(\frac{4}{3} - \frac{4}{3}v + v^2\right)\Delta_a^{in}$$

$$\Delta_a^{in} \approx \frac{1}{Z}\tilde{\Phi}_a^{in}(\delta) \quad \text{with} \quad \tilde{\Phi}_a^{in}(\delta) = \ln\left[\frac{\mu/\delta}{\delta\mu/m^2 + \sqrt{e}}\right] - \ln\left[1 + \frac{m}{\delta\sqrt{e}B'Z^{-2/3}}\right]$$

B'=1429 for $Z \geq 2$ and B'=446 for Z=1.

The maximum energy, transferred to the photon is

$$v_{max} = \frac{m(E - \mu)}{E(E - p + m)}$$

On the output all of the energy lost by a muon is assigned to the bremsstrahlung photon.

6.3 Photonuclear Interactions

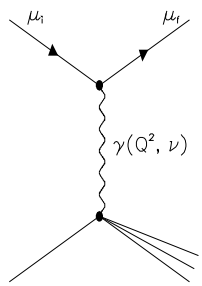

Photonuclear cross section is used as parametrized in [17]:

$$\begin{aligned}\frac{d\sigma}{dv} &= \frac{\alpha}{2\pi} A\sigma_{\gamma N} v \left\{ 0.75G(x)\left[\kappa \ln\left(1+\frac{m_1^2}{t}\right) - \frac{\kappa m_1^2}{m_1^2+t} - \frac{2\mu^2}{t}\right] + \right. \\ &+ \left. 0.25\left[\kappa \ln\left(1+\frac{m_2^2}{t}\right) - \frac{2\mu^2}{t}\right] + \frac{\mu^2}{2t}\left[0.75G(x)\frac{m_1^2}{m_1^2+t} + 0.25\frac{m_2^2}{t}\ln\left(1+\frac{t}{m_2^2}\right)\right]\right\}\end{aligned}$$

where $t = Q^2_{max} = \dfrac{\mu^2 v^2}{1-v}$, $\kappa = 1 - \dfrac{2}{v} + \dfrac{2}{v^2}$, $m_1^2 = 0.54$ GeV^2 , and $m_2^2 = 1.8$ GeV^2

Nucleon shadowing is taken care of by

$$\begin{aligned}\sigma_{\gamma A}(\nu) &= A\sigma_{\gamma N}(\nu)\{0.75G(x) + 0.25\} \\ \text{with } G(x) &= \frac{3}{x^3}\left(\frac{x^2}{2} - 1 + e^{-x}(1+x)\right), \quad \text{for } Z \neq 1, \text{ and } G(x) = 1 \text{ for Z=1} \\ x &= Rn\sigma_{\rho N} \simeq 0.00282 A^{\frac{1}{3}}\sigma_{\gamma N}(\nu)\end{aligned}$$

Several parametrization schemes for the photon-nucleon cross section are implemented. The first is

$$\begin{aligned}\sigma_{\gamma N}(\nu) &= 96.1 + \frac{82}{\sqrt{\nu}}, \quad \text{for } \nu \leq 17 \text{ GeV} \\ \sigma_{\gamma N}(\nu) &= 114.3 + 1.647\ln^2[0.0213\nu]\ \mu\text{b}, \quad \text{for } \nu \in [17, 200 \text{ GeV}] \ [17] \\ \sigma_{\gamma N}(\nu) &= 49.2 + 11.1\ln[\nu] + 151.8/\sqrt{\nu}\ \mu\text{b}, \quad \text{above 200 GeV} \ [18]\end{aligned}$$

The second is based on the table parametrization of [19] below 17 GeV. Since the second formula from above is valid for energies up to 10^6 GeV, it is taken to describe the whole energy range alone as the third case. Formula [20]

$$\sigma_{\gamma N}(\nu) = 63.5 s^{0.097} + 145 s^{-0.5}\ \mu\text{b} \quad \text{with} \quad s = 2M\nu$$

can also be used in the whole energy range, representing the forth case (see Fig. 18). Finally, the ALLM parametrization (discussed in Sec. 6.8) can be enabled. It does not rely on the assumption that the virtual photon can be considered as real and involves integration over the square of the photon 4-momentum (Q^2).

Integration limits used for the photonuclear cross section are (kinematic limits for Q^2 are used for the ALLM cross section)

$$\begin{aligned} m_\pi + \frac{m_\pi^2}{2M} &< \nu < E - \frac{M}{2}\cdot\left(1 + \frac{m_\mu^2}{M^2}\right) \\ \frac{m_\mu^2\nu^2}{EE'} - \frac{m_\mu^4}{2EE'} &< Q^2 < 2M(\nu - m_\pi) - m_\pi^2 \ , \quad E' = E - \nu \end{aligned}$$

6.4 Electron Pair Production Two out of four diagrams describing pair production are shown below. These describe the dominant "electron" term. The other two have muon interacting with the atom and represent the "muon" term. The cross section formulae used here were first derived in [21, 22, 23].

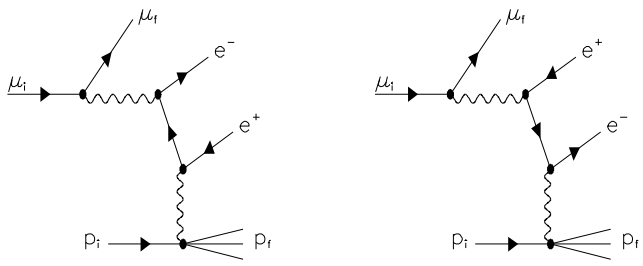

$$\frac{d\sigma(E,v,\rho)}{dv d\rho} = \frac{2}{3\pi} Z(Z+\zeta)(\alpha r_e)^2 \frac{1-v}{v}\left(\Phi_e + \frac{m^2}{\mu^2}\Phi_\mu\right)$$

$$v = (\epsilon_+ + \epsilon_-)/E, \quad \rho = (\epsilon_+ - \epsilon_-)/E$$

$$\begin{aligned}
\Phi_e &= \left\{[(2+\rho^2)(1+\beta) + \xi(3+\rho^2)]\ln\left(1+\frac{1}{\xi}\right) + \frac{1-\rho^2-\beta}{1+\xi} - (3+\rho^2)\right\} L_e \\
\Phi_\mu &= \left\{\left[(1+\rho^2)\left(1+\frac{3}{2}\beta\right) - \frac{1}{\xi}(1+2\beta)(1-\rho^2)\right]\ln(1+\xi) + \right. \\
&+ \left. \frac{\xi(1-\rho^2-\beta)}{1+\xi} + (1+2\beta)(1-\rho^2)\right\} L_\mu \\
L_e &= \ln\left(\frac{BZ^{-1/3}\sqrt{(1+\xi)(1+Y_e)}}{1+\frac{2m\sqrt{e}BZ^{-1/3}(1+\xi)(1+Y_e)}{Ev(1-\rho^2)}}\right) - \frac{1}{2}\ln\left[1+\left(\frac{3m}{2\mu}Z^{1/3}\right)^2(1+\xi)(1+Y_e)\right] \\
L_\mu &= \ln\left(\frac{\frac{2}{3}\frac{\mu}{m}BZ^{-2/3}}{1+\frac{2m\sqrt{e}BZ^{-1/3}(1+\xi)(1+Y_\mu)}{Ev(1-\rho^2)}}\right) \\
Y_e &= \frac{5-\rho^2+4\beta(1+\rho^2)}{2(1+3\beta)\ln(3+1/\xi) - \rho^2 - 2\beta(2-\rho^2)} \\
Y_\mu &= \frac{4+\rho^2+3\beta(1+\rho^2)}{(1+\rho^2)(3/2+2\beta)\ln(3+\xi) + 1 - \frac{3}{2}\rho^2}
\end{aligned}$$

$$\beta = \frac{v^2}{2(1-v)}, \quad \xi = \left(\frac{\mu v}{2m}\right)^2 \frac{1-\rho^2}{1-v}$$

$$\zeta_{loss}^{pair}(E,Z) \sim \frac{0.073\ln\left(\frac{E/\mu}{1+\gamma_1 Z^{2/3}E/\mu}\right) - 0.26}{0.058\ln\left(\frac{E/\mu}{1+\gamma_2 Z^{1/3}E/\mu}\right) - 0.14}$$

$$\begin{aligned}
\gamma_1 &= 1.95\ 10^{-5} \quad \text{and} \quad \gamma_2 = 5.3\ 10^{-5} \quad \text{for} \quad Z \neq 1 \\
\gamma_1 &= 4.4\ 10^{-5} \quad \text{and} \quad \gamma_2 = 4.8\ 10^{-5} \quad \text{for} \quad Z = 1
\end{aligned}$$

Integration limits for this cross section are

$$\begin{aligned} \frac{4m}{E} &= v_{min} \leq v \leq v_{max} = 1 - \frac{3\sqrt{e}}{4}\frac{\mu}{E}Z^{1/3} \\ 0 &\leq |\rho| \leq \rho_{max} = \sqrt{1-\frac{4m}{Ev}}\left[1-\frac{6\mu^2}{E^2(1-v)}\right] \end{aligned}$$

Muon pair production is discussed in detail in [24] and is not considered by MMC. Its cross section is estimated to be $\sim 2 \cdot 10^4$ times smaller than the direct electron pair production cross section discussed above.

6.5 Muon decay

Muon decay probability is calculated according to

$$\frac{dN}{dx} = \frac{1}{\gamma\beta c\tau}$$

The energy of the outgoing electron is evaluated as

$$\nu_e = \gamma\left(\nu_{rest} + \beta\sqrt{\nu_{rest}^2 - m_e^2}\cos(\theta)\right)$$

$\cos(\theta)$ is distributed uniformly on $(-1, 1)$ and ν_{rest} is determined at random from the distribution

$$\frac{dN}{dx} = \frac{G^2\mu^5}{192\pi^3}(3-2x)x^2, \quad x = \frac{\nu}{\nu_{max}} \quad \text{with} \quad \nu_{min} = m_e \quad \text{and} \quad \nu_{max} = \frac{\mu^2 + m_e^2}{2\mu}$$

6.6 Molière scattering

After passing through distance x angle distribution is assumed Gaussian with a width $\sqrt{2}\theta_0$ [11]

$$\theta_0 = \frac{13.6MeV}{\beta cp}z\sqrt{x/X_0}\,[1 + 0.038\ln(x/X_0)]$$

$$X_0 \quad \text{is evaluated as} \quad X_0 = \left[\frac{\sigma_{brems}(E_{big})}{E_{big}}\right]^{-1} \quad \text{for} \quad E_{big} \sim 10^{20}eV$$

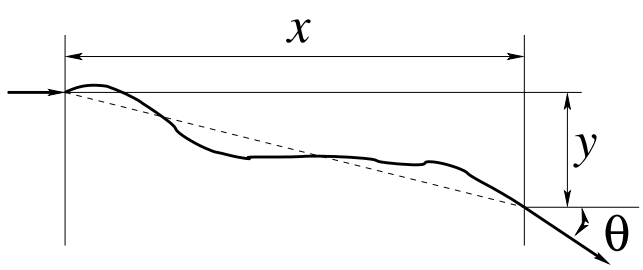

Deviations in two directions, perpendicular to the muon track are independent, but for each direction exit angle and actual deviation are correlated:

$$y_{plane} = z_1 x\theta_0/\sqrt{12} + z_2 x\theta_0/2 \quad \text{and} \quad \theta_{plane} = z_2\theta_0$$

for independent standard Gaussian random variables (z_1, z_2). A more precise treatment should take the finite size of nuclei into account as described in [25]. See Fig. 22 for an example of Molière scattering of a high energy muon.

6.7 Landau-Pomeranchuk-Migdal and Ter-Mikaelian effects

These affect bremsstrahlung and pair production. See Fig. 21 for the combined effect in ice and Fréjus rock.

6.7.1 LPM suppression of the bremsstrahlung cross section Bremsstrahlung cross section is modified as follows [26, 27, 28]:

$$\frac{4}{3}(1-v)+v^2 \to \frac{\xi(s)}{3}\left(v^2 G(s) + 2[1+(1-v)^2]\phi(s)\right)$$

The regions of the following expressions for $\phi(s)$ and $G(s)$ were chosen to represent the best continuous approximation to the actual functions.

$$\begin{aligned}
\phi(s) &= 1-\exp\left(-6s\left[1+(3-\pi)s\right]+\frac{s^3}{0.623+0.796s+0.658s^2}\right) \quad \text{for} \quad s<1.54954 \\
\phi(s) &= 1-0.012/s^4 \quad \text{for} \quad s \geq 1.54954 \\
\psi(s) &= 1-\exp\left(-4s-\frac{8s^2}{1+3.936s+4.97s^2-0.05s^3+7.50s^4}\right) \\
G(s) &= 3\psi(s)-2\phi(s) \quad \text{for} \quad s<0.710390 \\
G(s) &= 36s^2/(36s^2+1) \quad \text{for} \quad 0.710390 \leq s < 0.904912 \\
G(s) &= 1-0.022/s^4 \quad \text{for} \quad s \geq 0.904912
\end{aligned}$$

Here the SEB scheme [29] is employed for evaluation of $\phi(s)$ and $\psi(s)$ and $\xi(s)$ below:

$$\begin{aligned}
\xi(s') &= 2 \quad \text{for} \quad s'<s_1 \\
\xi(s') &= 1+h-\frac{0.08(1-h)[1-(1-h)^2]}{\ln s_1} \quad \text{for} \quad s_1 \leq s' < 1 \\
\xi(s') &= 1 \quad \text{for} \quad s' \geq 1
\end{aligned}$$

$$E_{LPM} = \frac{\alpha(\mu c^2)^2 X_0}{4\pi\hbar c}$$

X_0 is the same as in Sec. 6.6. Here are the rest of the definitions:

$$s=\frac{s'}{\sqrt{\xi}} \quad s_1=\sqrt{2}\frac{Z^{1/3}D_n}{B}\frac{m_e}{\mu} \quad s'=\sqrt{\frac{E_{LPM}v}{8E(1-v)}} \quad h=\frac{\ln s'}{\ln s_1}$$

6.7.2 Dialectric (Longitudinal) suppression effect In addition to the above change of the bremsstrahlung cross section, s is replaced by $\Gamma \cdot s$ and functions $\xi(s)$, $\phi(s)$ and $G(s)$ are scaled as [28]

$$\xi(s) \to \xi(\Gamma s) \quad \phi(s) \to \phi(\Gamma s)/\Gamma \quad G(s) \to G(\Gamma s)/\Gamma^2$$

Therefore the first formula in the previous section is modified as

$$\frac{4}{3}(1-v)+v^2 \to \frac{\xi(\Gamma s)}{3}\left(v^2\frac{G(\Gamma s)}{\Gamma^2}+2[1+(1-v)^2]\frac{\phi(\Gamma s)}{\Gamma}\right)$$

$$\Gamma \quad \text{is defined as} \quad \Gamma = 1+\gamma^2\left(\frac{\hbar\omega_p}{vE}\right)^2$$

where $\omega_p = \sqrt{4\pi N Z e^2/m}$ is plasma frequency of the medium and vE is the photon energy. The dialectric suppression affects only processes with small photon transfer energy, therefore it is not directly applicable to the direct pair production suppression.

6.7.3 LPM suppression of the direct pair production cross section

Φ_e from the pair production cross section is modified as follows [28, 30]:

$$\Phi_e \to \big((1+\beta)(A+[1+\rho^2]B)+\beta(C+[1+\rho^2]D)+(1-\rho^2)E\big)\cdot L_e$$

$$s=\frac{1}{4}\sqrt{\frac{E_{LPM}}{E_\mu}\frac{1}{v(1-\rho^2)}}$$

E_{LPM} energy definition is different than in the bremsstrahlung case:

$$E_{LPM}=\frac{\mu^4}{2\pi n\alpha^2\sum Z^2 L} \quad \text{where} \quad L=\ln(3.25BZ^{-1/3})$$

Functions $A(s,\xi)$, $B(s,\xi)$, $C(s,\xi)$ and $D(s,\xi)$ are based on the approximation formulae

$$\Phi(s)=\frac{6s}{6s+1} \quad \text{and} \quad G(s)=\frac{(6s)^2}{(6s)^2+1}$$

and are given below

$$A(s,x)=\frac{G}{2}(1+2Gx)\ln\frac{36s^2(1+x)^2+1}{36s^2x^2}-G+6Gs\left(1+\frac{36s^2-1}{36s^2+1}x\right)\left(\arctan(6s[x+1])-\frac{\pi}{2}\right)$$

$$B(s,x)=\Phi(1+\Phi x)\ln\frac{6s(1+x)+1}{6sx}-\Phi$$

$$C(s,x)=-G^2x\ln\frac{36s^2(1+x)^2+1}{36s^2x^2}+G-\frac{G^2(36s^2-1)}{6s}x\left(\arctan(6s[x+1])-\frac{\pi}{2}\right)$$

$$D(s,x)=\Phi-\Phi^2x\ln\frac{6s(1+x)+1}{6sx}$$

$$E(s,x)=-6s\left(\arctan(6s[x+1])-\frac{\pi}{2}\right)$$

6.8 The Abramowicz Levin Levy Maor (ALLM) parametrization of the photonuclear cross section

The ALLM formula is based on the parametrization [31, 32, 33]

$$\frac{d\sigma(v,Q^2)}{dvdQ^2}=\frac{4\pi\alpha^2}{Q^4}\frac{F_2}{v}\left[1-v-\frac{Mxv}{2E}+\left(1-\frac{2\mu^2}{Q^2}\right)\frac{v^2(1+4M^2x^2/Q^2)}{2(1+R))}\right]$$

$$x=\frac{Q^2}{2MEv}$$

The limits of integration over Q^2 are given in the section for photonuclear cross section.

$$F_2=a(Z+(A-Z)P)F_2^p \quad \text{Here} \quad a(A,x,Q^2)\simeq a(A,x)$$

$$\begin{aligned}
a(A,x) &= A^{-0.1} \quad \text{for} \quad x<0.0014\\
a(A,x) &= A^{0.069\log_{10}x+0.097} \quad \text{for} \quad 0.0014\le x<0.04\\
a(A,x) &= 1 \quad \text{for} \quad x\ge 0.04
\end{aligned}$$

$$F_2^p(x,Q^2) = \frac{Q^2}{Q^2+m_0^2}(F_2^P + F_2^R)$$

$$F_2^i(x,Q^2) = c_i x_i^{a_i}(1-x)^{b_i} \quad \text{for} \quad i = P, R$$

$$\text{For} \quad f = c_R, a_R, b_R, b_P \qquad f(t) = f_1 + f_2 t^{f_3}$$

$$\text{For} \quad g = c_P, a_P \qquad g(t) = g_1 + (g_1 - g_2)\left[\frac{1}{1+t^{g_3}} - 1\right]$$

$$t = \ln \frac{\ln \frac{Q^2+Q_0^2}{\Lambda^2}}{\ln \frac{Q_0^2}{\Lambda^2}}$$

$$x_i = \frac{Q^2+m_i^2}{Q^2+m_i^2+W^2-M^2} \quad \text{for} \quad i = P, R$$

W is the invariant mass of the nucleus plus virtual photon [34]: $W^2 = M^2 + 2MEv - Q^2$. Fig. 19 compares ALLM-parametrized cross section with formulae of Bezrukov and Bugaev from Sec. 6.3.

$R(x,Q^2)$ is not very well known, although it has been measured for high x ($x > 0.1$) [35] and modeled for small x ($10^{-7} < x < 0.1$, $0.01\text{GeV}^2 < Q^2 < 50\text{GeV}^2$) [36]. It is of the order $\sim 0.1 - 0.3$ and even smaller for small Q^2 (behaves as $O(Q^2)$). In the Fig. 20 three photonuclear energy loss curves for R=0, 0.3 and 0.5 are shown. The difference between the curves never exceeds 7%. In the absence of a convenient parametrization for R at the moment, it is set to zero in MMC.

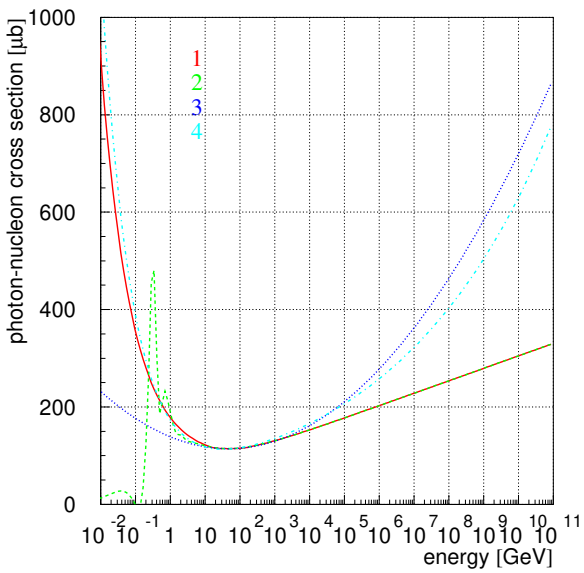

Fig. 18: photon-nucleon cross sections, as described in the text (Bezrukov Bugaev parametrization): 1 (solid), 2 (dashed), 3 (dotted), 4(dashed-dotted)

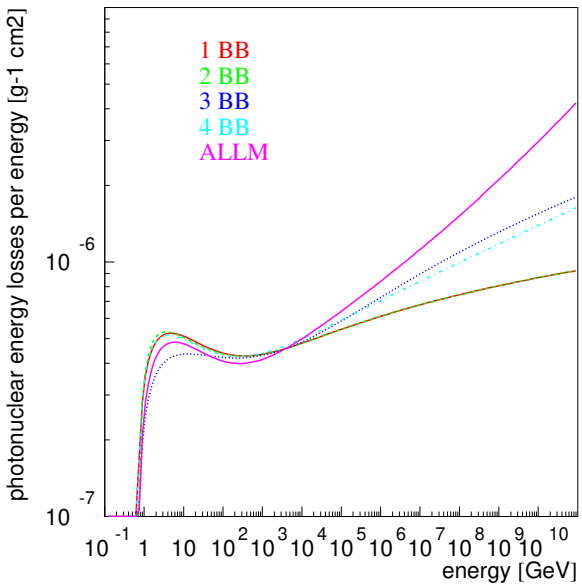

Fig. 19: photonuclear energy losses (divided by energy), according to different formulae. Designations are the same as in Fig. 18, higher solid line is for ALLM parametrization

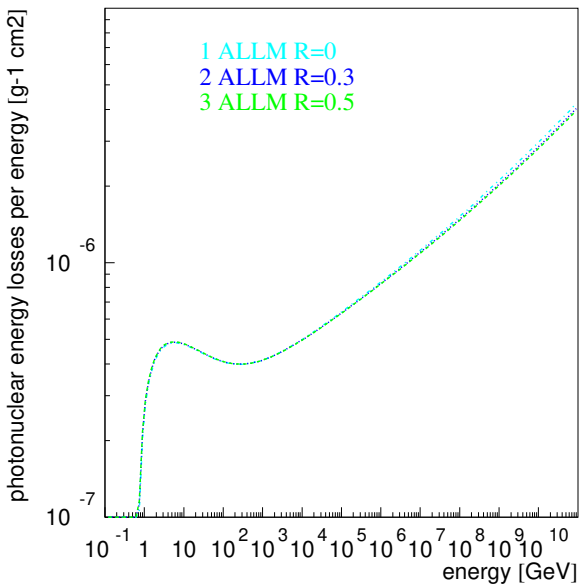

Fig. 20: comparison of ALLM energy loss (divided by energy) for R=0 (dashed-dotted), R=0.3 (dotted), R=0.5 (dashed)

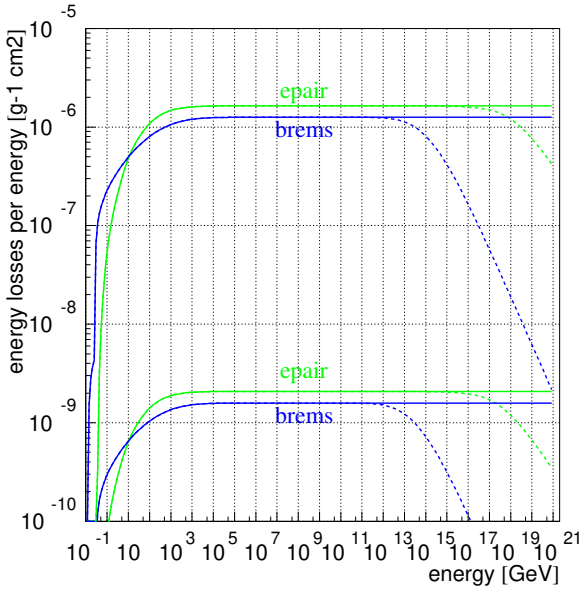

Fig. 21: LPM effect in ice (higher plots) and Fréjus rock (lower plots, multiplied by 10^{-3})

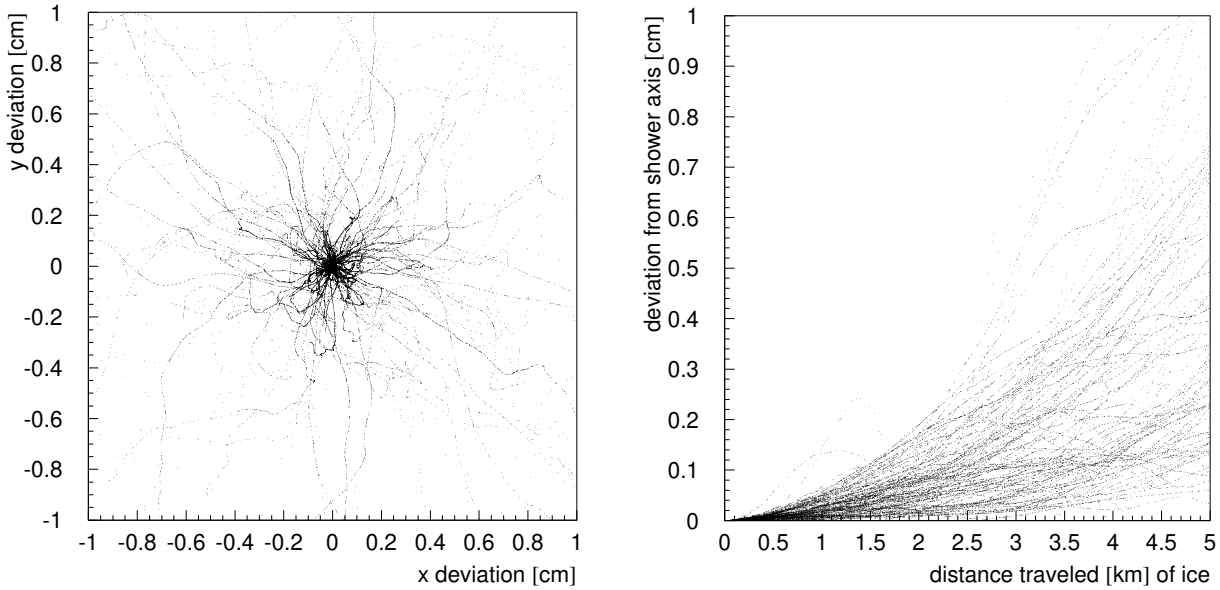

Fig. 22: Molière scattering of 100 10 TeV muons going straight down through ice

7 Tables

All cross sections were translated to units $[1/cm]$ via multiplying by number of molecules per volume. Unit conversions (like eV $\rightarrow$ J) were achieved using values of $\alpha = e^2/\hbar c$ and $r_e = e^2/m_e c^2$.

7.1 Summary of physical constants employed by MMC

α	1/137.03599976	r_e	$2.817940285 \cdot 10^{-13}$ cm
N_a	$6.02214199 \cdot 10^{23}$ 1/mol	K	0.307075 $MeV \cdot cm^2/g$
c	$299792458 \cdot 10^{10}$ cm/s	R_y	13.60569172 eV
m_e	0.510998902 MeV	m_π	139.57018 Mev
m_p	938.271998 MeV	m_n	939.56533 MeV
m_μ	105.658389 MeV	τ_μ	$2.19703 \cdot 10^{-6}$ s
m_τ	1777.03 MeV	τ_τ	$290.6 \cdot 10^{-15}$ s

7.2 Media constants

Material	Z	A	I, eV	C	a	m	X_0	X_1	ρ, g/cm^2
Water	1 +	1.00794	75.0	-3.5017	0.09116	3.477	0.240	2.8004	1.000
Ice	+ 8	15.9994	75.0	-3.5017	0.09116	3.477	0.240	2.8004	0.917
Stand. Rock	11	22	136.4	-3.774	0.083	3.412	0.049	3.055	2.650
Fréjus Rock	10.12	20.34	149.0	-5.053	0.078	3.645	0.288	3.196	2.740
Iron	26	55.845	286.0	-4.291	0.147	2.963	-0.001	3.153	7.874
Hydrogen	1	1.00794	21.8	-3.263	0.135	5.625	0.476	1.922	0.063
Lead	82	207.200	823.0	-6.202	0.094	3.161	0.378	3.807	11.350
Uranium	92	238.0289	890.0	-5.869	0.197	2.817	0.226	3.372	18.950

7.3 Radiation logarithm constant B (taken from [37])

Z	B	Z	B	Z	B	Z	B	Z	B
1	202.4	8	173.4	15	172.2	22	176.8	53	178.6
2	151.9	9	170.0	16	173.4	26	175.8	74	177.6
3	159.9	10	165.8	17	174.3	29	173.1	82	178.0
4	172.3	11	165.8	18	174.8	32	173.0	92	179.8
5	177.9	12	167.1	19	175.1	35	173.5		
6	178.3	13	169.1	20	175.6	42	175.9	other	182.7
7	176.6	14	170.8	21	176.2	50	177.4		

7.4 ALLM parameters (as in [32, 38])

a_{P1}	-0.0808	a_{P2}	-0.44812	a_{P3}	1.1709
a_{R1}	0.58400	a_{R2}	0.37888	a_{R3}	2.6063
b_{P1}	0.60243^2	b_{P2}	1.3754^2	b_{P3}	1.8439
b_{R1}	0.10711^2	b_{R2}	1.9386^2	b_{R3}	0.49338
c_{P1}	0.28067	c_{P2}	0.22291	c_{P3}	2.1979
c_{R1}	0.80107	c_{R2}	0.97307	c_{R3}	3.4942
m_P^2	$49.457 \cdot 10^6$ MeV^2	Λ^2	$0.06527 \cdot 10^6$ MeV^2	m_0^2	$0.31985 \cdot 10^6$ MeV^2
m_R^2	$0.15052 \cdot 10^6$ MeV^2	$Q_0^2 - \Lambda^2$	$0.46017 \cdot 10^6$ MeV^2		

References

[1] Andres, E. et al. (AMANDA Collaboration), Nature (2001) 441

[2] DeYoung, Tyce R., Dissertation, U. of Wisconsin-Madison, 2001

[3] Heck, D. et al., Report FKZA 6019, 1998

[4] Chirkin, D., Rhode, W., 26th ICRC, HE 3.1.07 Salt Lake City, 1999

[5] Desiati, P., Rhode, W., 27th ICRC, HE 205 Hamburg, 2001

[6] Numerical Recipes (W. H. Press, B. P. Flannery, S. A. Teukolsky, W. T. Vetterling)

[7] Rhode, W., Cârloganu, C., DESY-PROC-1999-01, 1999

[8] Bugaev, E., Sokalski, I., Klimushin, S., hep-ph/0010322, hep-ph/0010323, 2000

[9] Schröder, F., Rhode, W., Meyer, H., 27th ICRC, HE 2.2 Hamburg, 2001

[10] Winterer, V.-H., SYMPHONY (talk)

[11] The Europen Physics Journal C vol. 15, pp 163-173, 2000

[12] Rossi, B., High Energy Particles, Prentice-Hall, Inc., Englewood Cliffs, NJ, 1952

[13] S.R. Kelner, R.P. Kokoulin, A.A. Petrukhin, About Cross Section for High Energy Muon Bremsstrahlung, Preprint of Moscow Engineering Physics Inst., Moscow, 1995, no 024-95.

[14] Bethe, H., Heitler, W, Proc. Roy. Soc., A146, 83 (1934)

[15] Bethe, H., Proc. Cambr. Phil. Soc., 30, 524 (1934)

[16] S.R. Kelner, R.P. Kokoulin, A.A. Petrukhin, Bremsstrahlung from Muons Scattered by Atomic Electrons, Physics of Atomic Nuclei, Vol 60, No 4, 1997, 576-583.

[17] L.B. Bezrukov and E.V. Bugaev, Nucleon shadowing effects in photonuclear interactions, Sov. J. Nucl. Phys. 33(5), May 1981.

[18] R.P. Kokoulin, Nucl. Phys. B (Proc. Suppl.) 70 (1999) 475-479.

[19] W. Rhode, Diss. Univ. Wuppertal, WUB-DIS- 93-11 (1993); W. Rhode, Nucl. Phys. B. (Proc. Suppl.) 35 (1994), 250-253

[20] ZEUS Collaboration, Z. Phys. C, 63 (1994) 391.

[21] S.R. Kelner, Yu.D. Kotov, Muon energy loss to pair production, Soviet Journal of Nuclear Physics, Vol 7, No 2, 237, (1968).

[22] R.P. Kokoulin, A.A. Petrukhin, Analysis of the cross section of direct pair production by fast muons, Proc. 11th Int. Conf. on Cosmic Ray, Budapest 1969.

[23] R.P. Kokoulin, A.A. Petrukhin, Influence of the nuclear form factor on the cross section of electron pair production by high energy muons, Proc. 12th Int. Conf. on Cosmic Rays, Hobart 6 (1971), A 2436.

[24] Kelner, S., Kokoulin, R., Petrukhin, A., Direct Production of Muon Pairs by High-Energy Muons, Phys. of Atomic Nuclei, Vol. 63, No 9 (2000) 1603

[25] Butkevitch, A., Kokoulin, R., Matushko, G., Mikheyev, S., Comments on multiple scattering of high-energy muons in thick layers, hep-ph/0108016, 2001

[26] Klein, S., Suppression of bremsstrahlung and pair production due to environmental factors, Rev. Mod. Phys., Vol 71, No 5 (1999) 1501

[27] Migdal, A., Bremsstrahlung and Pair Production in Condensed Media at High Energies Phys. Rev., Vol. 103, No 6 (1956) 1856

[28] Polityko, S., Takahashi, N., Kato, M., Yamada, Y., Misaki, A., Muon's Behaviors under Bremsstrahlung with both the LPM effect and the Ter-Mikaelian effect and Direct Pair Production with the LPM effect, hep-ph/9911330, 1999

[29] Stanev, T., Vankov, Ch., Streitmatter, R., Ellsworth, R., Bowen, T., Development of ultrahigh-energy electromagnetic cascades in water and lead including the Landau-Pomeranchuk-Migdal effect Phys. Rev. D 25 (1982) 1291

[30] Ternovskii, F., Effect of multiple scattering on pair production by high-energy particles in a medium, Sov. Phys. JETP, Vol 37(10), No 4 (1960) 718

[31] Abramowicz, H, Levin, E., Levy, A., Maor, U., A parametrization of $\sigma_T(\gamma^* p)$ above the resonance region for $Q^2 \geq 0$, Phys. Lett. B269 (1991) 465

[32] Abramowicz, H., Levy, A., The ALLM parametrization of $\sigma_{tot}(\gamma^* p)$ an update, hep-ph/9712415, 1997

[33] Dutta, S., Reno, M., Sarcevic, I., Seckel, D., Propagation of Muons and Taus at High Energies, hep-ph/0012350, 2000

[34] Badelek, B., Kwiencinski, J., The low-Q^2, low-x region in electroproduction, Rev. Mod. Phys. Vol 68 No 2 (1996) 445

[35] Whitlow, L., Rock, S., Bodek, A., Dasu, S., Riordan, E., A precise extraction of $R = \sigma_L/\sigma_T$ from a global analysis of the SLAC deep inelastic e-p and e-d scattering cross sections, Phys. Lett. B250 No1,2 (1990) 193

[36] Badelek, B., Kwiecinski, J., Stasto, A., A model for F_L and $R = F_L/F_T$ at low x and low Q^2, Z. Phys. C 74 (1997) 297

[37] Kelner, S., Kokoulin, R, Petrukhin, A., Radiation Logarithm in the Hartree-Fock Model, Phys. of Atomic Nuclei, Vol. 62, No. 11, (1999) 1894

[38] Abramowicz, H., private communication